

# A Hetero-Bifunctional Spacer for the Smart Engineering of Carbon-Based Nanostructures

Giulia Tuci,<sup>[a]</sup> Lapo Luconi,<sup>[a]</sup> Andrea Rossin,<sup>[a]</sup> Francesco Baldini,<sup>[b]</sup> Stefano Cicchi,<sup>[c]</sup> Sara Tombelli,<sup>[b]</sup> Cosimo Trono,<sup>[b]</sup> Ambra Giannetti,<sup>[b]</sup> Ilse Manet,<sup>[d]</sup> Stefano Fedeli,<sup>[c]</sup> Alberto Brandi,<sup>[c]</sup> and Giuliano Giambastiani<sup>\*[a, e]</sup>

*Dedicated to Professor Max Malacria on the occasion of his 65th birthday*

Efforts have been made in recent years to develop novel functionalisation protocols aimed at imparting multimodality and improved properties to complex carbon-based nanostructures. The incorporation of cleavable bonds to the nanomaterial surface for the controlled release (or exchange) of specific molecules under appropriate chemical and biological settings is relatively unexplored. The design and synthesis of a hetero-bifunctional linker joining a “cleavable” disulfide moiety for the covalent anchoring of a wide range of thiol end-capped (bio)-

molecules and a “clickable” terminal acetylene group is described. The strategy is based on the well-established copper-mediated acetylene–azide coupling reaction between the acetylene linker and single-walled carbon nanotubes decorated with phenylazido pendant arms. As a result, easily “post-derivatisable” and traceable nanostructured platforms containing a linking group potentially available for a wide range of biological probes are prepared and completely characterised.

## Introduction

Many efforts have been devoted in the last two decades to the development of effective and simple functionalisation schemes for 1D and 2D carbon nanostructures with the final aim of improving their processability and handling as well as imparting multimodality to the resulting hybrids.<sup>[1]</sup> In particular, carbon nanotubes (CNTs) have been widely explored as substrates for a number of functionalisation protocols to afford decorated nanostructured systems with unique physicochemical properties.<sup>[2]</sup> Potential applications of the as-prepared CNT-based hybrids are envisaged in different technological fields: from the preparation of nanocomposite materials with improved properties<sup>[3]</sup> and their exploitation in nanomedicine for drug delivery,<sup>[4]</sup> therapy and imaging,<sup>[5]</sup> to their use as catalytic materials

in specific fields of renewable energies technology.<sup>[6]</sup> In spite of a number of well-established CNT functionalisation protocols,<sup>[7]</sup> the development of new synthetic methodologies that lead to a more efficient integration of these nanomaterials into complex functional structures still represents a challenging research matter in the field. In particular, the incorporation of functionalities containing cleavable bonds (under appropriate chemical and/or biological settings) is a step forward towards the smart engineering of these nanostructures.<sup>[8]</sup> Controlled molecular exchange at the CNT surface is still a relatively unexplored field, although it can offer a unique strategy for the controlled release of specific guest molecules initially linked to the surface of the nanomaterial carrier (CNT). For instance, Dai and co-workers demonstrated how the intracellular delivery of CNT-based bioconjugates and the subsequent release of the biological probe from the nanocarrier (CNT) could be triggered by a selective disulfide bond cleavage operated by thiol-reducing enzymes.<sup>[9]</sup> Similarly, You et al. demonstrated how chemically decorated CNTs could easily conjugate and release biological molecules at will, according to specific biological or chemical stimuli.<sup>[10]</sup> Both technologies conceptually lie on the design and synthesis of a “cleavable” linker for the covalent anchoring of a wide range of thiol end-capped biomolecules (including DNA, RNA and proteins).

Some of us recently reported the preparation of flexible and versatile “CNT platforms” chemoselectively decorated with aryl-azido pendant arms;<sup>[11]</sup> their exploitation, in combination with variably substituted terminal acetylenes (or mixtures thereof), under classical bio-orthogonal copper-mediated acetylene–azide coupling (CuAAC) conditions,<sup>[12]</sup> has provided a valuable

[a] Dr. G. Tuci, Dr. L. Luconi, Dr. A. Rossin, Dr. G. Giambastiani  
Institute of Chemistry of OrganoMetallic Compounds, ICCOM-CNR  
Via Madonna del Piano, 10, 50019 Sesto F.no, Florence (Italy)  
Fax: (+39) 055-5225203  
E-mail: giuliano.giambastiani@iccom.cnr.it

[b] Dr. F. Baldini, Dr. S. Tombelli, Dr. C. Trono, Dr. A. Giannetti  
Institute of Applied Physics, IFAC-CNR  
Via Madonna del Piano, 10  
50019 Sesto F.no (Florence) (Italy)

[c] Prof. S. Cicchi, Dr. S. Fedeli, Prof. A. Brandi  
Chemistry Department, University of Florence  
Via della Lastruccia 3–13, 50019 Sesto F.no, Florence (Italy)

[d] Dr. I. Manet  
Institute for the Organic Synthesis and Photoreactivity, ISOF-CNR  
Via Gobetti 101, 40129 Bologna (Italy)

[e] Dr. G. Giambastiani  
Kazan Federal University, 420008 Kazan (Russian Federation)

Supporting information for this article is available on the WWW under <http://dx.doi.org/10.1002/cplu.201402391>.

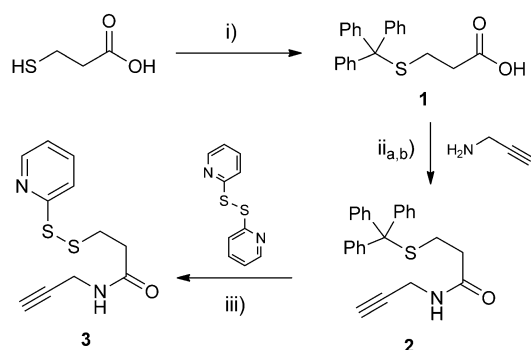
protocol for a controlled single-step homo- and hetero-functionalisation of the single-walled carbon nanotube (SWCNT) side walls.<sup>[13]</sup> Herein, the easy-to-scale-up synthesis of a simple organic linker joining a cleavable disulfide moiety and a “clickable” terminal acetylene group is described. Its chemistry is fully investigated in the homogeneous phase by means of model reaction protocols before being clicked at the surface of the above-mentioned phenylazido-functionalized SWCNT platforms ( $f_{N3}$ -SWCNT). The data reported hereafter describe a functionalisation scheme capable of imparting multimodality (i.e., multifunctionality) to 1D carbon nanostructures, while they operate as nanocarriers for potential biological probes. The CNT conjugation with thiol end-capped biomolecules is conveniently followed spectroscopically by monitoring the appearance of a characteristic absorbance band(s) owing to the release in solution of pyridine-2-thiol (or pyridine-2-thione) as the side product(s). Simple UV/Vis measurements allow for a precise estimation of the loading of the biomolecules covalently grafted on the CNT, and appropriate hetero-decoration of the nanomaterial with a selected fluorescence dye (boron dipyrromethene (BODIPy) derivative) generates an optically traceable bioconjugate. In addition, this study offers interesting insights on the role of the grafted molecules on the ultimate material morphology, while providing clear evidence of the distribution of the phenylazido groups at the CNT surface as a consequence of the aryldiazonium salt regiochemistry.

## Results and Discussion

### Synthesis of the hetero-bifunctional spacer 3

The approach to this study starts with the gram-scale synthesis of the hetero-bifunctional cross-linker **3**. Scheme 1 illustrates the stepwise procedure developed to prepare the desired acetylene derivative in good yield (51% over three steps).

According to this synthetic pathway, the 3-tritylsulfanylpropanamide **2** is straightforwardly prepared through an initial sulfhydryl trityl protection of the commercially available 3-mercaptopropionic acid followed by a one-pot activation/amidation of the carboxylic acid (DCC, HOBt, propargylamine) to



**Scheme 1.** Synthesis of the acetylene spacer **3**. Reagents and conditions: i)  $\text{Ph}_3\text{CCl}$ ,  $\text{CH}_2\text{Cl}_2$ , RT, overnight;<sup>[14]</sup> ii<sub>a</sub>) dicyclohexylcarbodiimide (DCC), 1-hydroxybenzotriazole (HOBt), DMF, RT, 3 h; ii<sub>b</sub>) propargylamine,  $\text{Et}_3\text{SiH}$ , DMF, 24 h; iii) 1,2-di(pyridin-2-yl)disulfane (2-aldrithiol),  $\text{Et}_3\text{SiH}$ , trifluoroacetic acid (TFA),  $\text{CH}_2\text{Cl}_2$ , RT, 5 h.

give the acetylene intermediate as a white solid in 82% yield over two steps. At odds with several literature precedents,<sup>[14–17]</sup> all of our attempts to obtain the free alkylthiol intermediate by sulfhydryl deprotection of isolated **2** failed. Indeed, the reaction of **2** with  $\text{Et}_3\text{SiH}$  and TFA gave, upon solvent evaporation, only untreatable rubbery materials. On the contrary, the one-pot addition<sup>[18]</sup> of the 2-aldrithiol reagent to a solution of **2** in  $\text{CH}_2\text{Cl}_2$ , followed by treatment with  $\text{Et}_3\text{SiH}$  and TFA, gives the desired product **3** as a viscous pale yellow oil in 62% yield after chromatographic purification.

### Reactivity study on the hetero-bifunctional cross-linker **3** in the homogeneous phase

Before applying **3** to the homo- and hetero-decoration of complex carbon nanostructures, the reactivity of its terminal functionalities was scrutinised and optimised in the homogeneous phase in combination with model reactants. To verify the reactivity at the disulfide linkage in **3**, a solution of dithiothreitol (DTT) was added to cleave and reduce the disulfide bridge, leading to the free sulfhydryl derivative **4** with the simultaneous release of one equivalent of pyridine-2-thione (**5**). The reaction was performed in a 25:75 mixture of DMF/phosphate buffered saline (PBS) at pH 7.2, in which cleavage proceeds quantitatively. DMF is used to improve the solubility of **3** and the reaction course is conveniently followed by UV/Vis measurements.

Two solutions at different concentration of **3** ( $1 \times 10^{-4}$  and  $5 \times 10^{-5}$  M) have been prepared and treated with DTT. The UV/Vis measurements on the solutions before (blank samples, dashed lines in Figure 1A) and after treatment with DTT (solid lines in Figure 1A), show the appearance of a clear absorbance band at  $\lambda = 343$  nm, which is typical of the pyridine-2-thione moiety, the intensity of which is proportional to the extent of disulfide cleavage (see the Experimental Section for more details).

According to the UV/Vis measurements, for both solutions, quantitative disulfide cleavage takes place at room temperature within a few minutes. Optimised CuAAC conditions have also been setup in the homogeneous phase between the terminal acetylene moiety on **3** and the model BODIPy phenylazido derivative **6**. Different copper(I)/copper(II)-based catalysts have been systematically scrutinised under classical reaction protocols to afford the cycloaddition product in good yields. Among these, both  $\text{CuSO}_4$ /sodium ascorbate/DMF and  $(\text{EtO})_3\text{P-CuI}$ /DMF gave almost identical yields, whereas other soluble  $\text{Cu}^I$  sources, such as  $\text{CuI}/1,5$ -diazabicyclo[5.4.0]undec-5-ene (DBU)/DMF, resulted in lower yields of **7**. A fluorescence study was performed on **6** before and after the CuAAC reaction (to give **7**) to assess the effect of the triazole linker on the dye fluorescence emission properties. As shown in Figure 1B, the fluorescence of the dye is invariably maintained in the cycloaddition product **7**.<sup>[19]</sup> Finally, cleavage of the disulfide bridge was quantitatively achieved at room temperature in a few minutes upon treatment with TDT (Scheme 2). The scant solubility of **7** in protic media requires a modification of the cleavage conditions as well as the use of more lipophilic TDT. The reaction

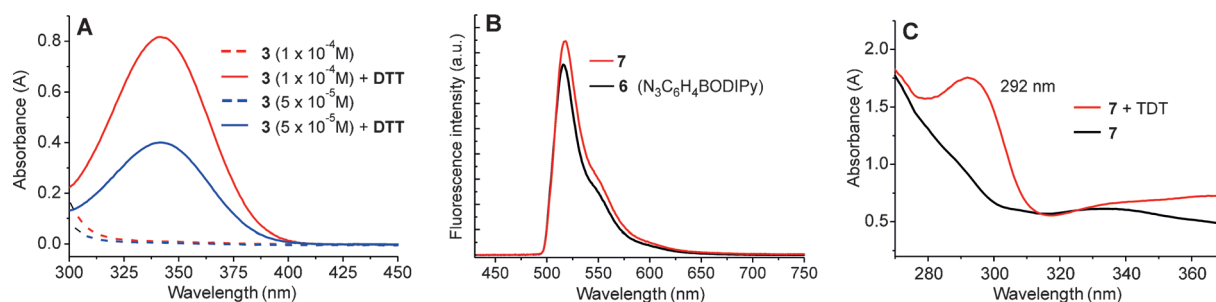
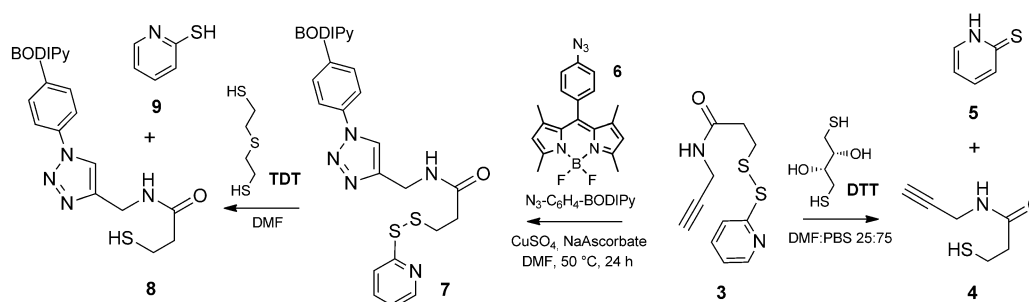


**Figure 1.** A) UV/Vis measurements on solutions of **3** at different concentrations before and after treatment with DTT (20-fold excess). B) Fluorescence measurements on **6** before and after CuAAC reaction (to give **7**); the excitation scattering light was eliminated by means of a long-pass filter setup (cut-on  $\lambda = 500$  nm, see the Experimental Section for more information). C) UV measurements on a solution of **7** before and after treatment with 2,2'-thiodiethanethiol (TDT; 20-fold excess).



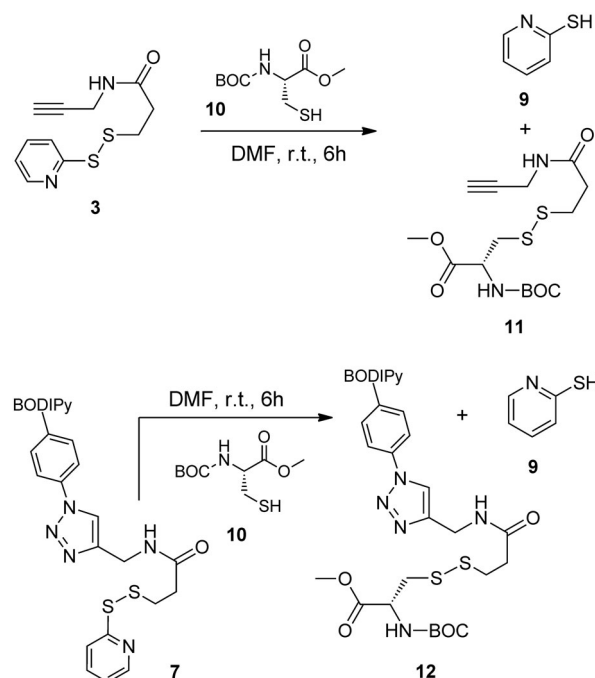
**Scheme 2.** Reactivity tests on the hetero-bifunctional cross-linker **3**. Optimised conditions for S–S cleavage and the CuAAC reaction in the homogeneous phase.

was performed in pure DMF and the process was systematically followed by UV measurements. A clear absorbance band at  $\lambda = 292$  nm, owing to the preferred pyridine-2-thiol isomer (**9**) in aprotic solvents,<sup>[20]</sup> was observed, without any interference with the absorbance wavelengths of the BODIPy dye (Figure 1C).

For the sake of completeness, both the spacer **3** and the intermediate **7** were reacted with the protected natural L-amino acid **10** (*N*-(*tert*-butoxycarbonyl)-L-cysteine methyl ester), which was selected as a mimic of a sulfhydryl-terminating residue of a more complex protein chain (Scheme 3). In both systems, the reaction with **10** proceeds smoothly, leading to complete conjugation of the protected L-amino acid through the disulfide bond after stirring the mixture in DMF at RT over 6 h. Similarly to the results reported above, the reaction course was followed spectroscopically until completion was determined by monitoring the appearance of the absorbance at  $\lambda = 292$  nm owing to the generation of the pyridine-2-thiol species (**9**). Reaction workup and chromatographic purification of the crude mixtures gave the conjugated compounds **11** and **12** in 62 and 39% yield, respectively.

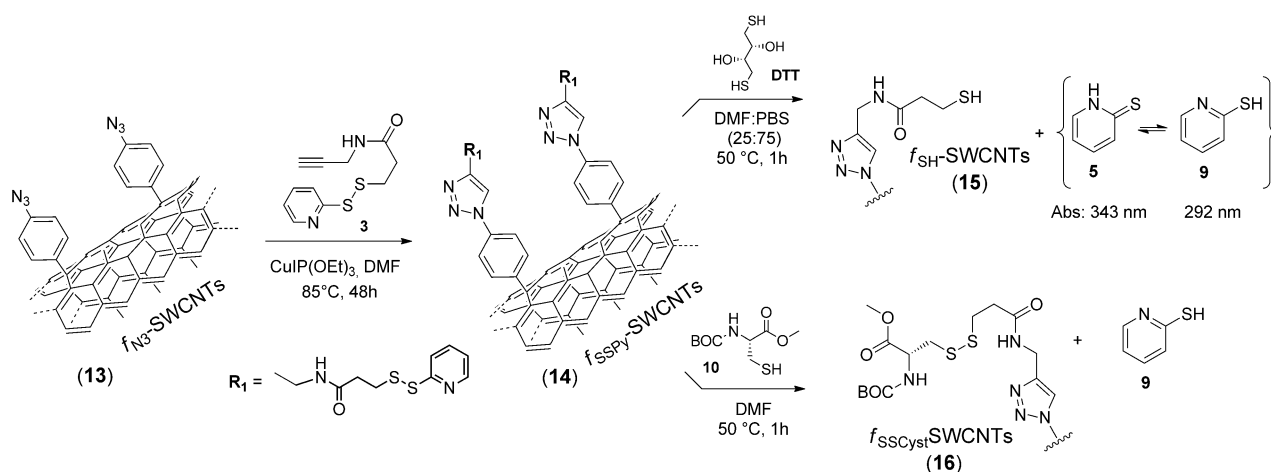
### Homo- and hetero-decoration of $f_{N_3}$ -SWCNTs: Towards multi-functional CNT platforms

As a natural step forward towards the covalent homo- and hetero-decoration of complex carbon nanostructures, the hetero-bifunctional cross-linker **3** was employed in combination with state-of-the-art CNT platforms decorated with arylazi-



**Scheme 3.** Reaction of model sulfhydryl-terminating amino acid **10** on **3** and **7**, and isolation of the respective conjugated compounds **11** and **12**. BOC = *tert*-butoxycarbonyl.

do pendant arms. The exploited post-functionalisation methodology relies on the preliminary covalent anchoring of **3** to the CNT side walls by using the CuAAC protocol (Scheme 4).



**Scheme 4.** The CuAAC reaction between the arylazido-decorated **13** and the alkyne-terminated spacer **3**. Post-derivatization of intermediate **14** by either disulfide cleavage (**14**→**15**) or conjugation with a HS-terminating amino acid residue of a model protein chain (**14**→**16**).

In a typical procedure, compound **3** and the  $f_{N_3}$ -SWCNTs (**13**) are reacted in degassed DMF at 85 °C for 2 days in the presence of a catalytic amount (10 mol% respect to **3**) of the soluble Cu<sup>I</sup> source CuI[P(OEt)<sub>3</sub>]. No appreciable changes (in terms of either chemical conversion or workup/purification procedures) were observed when the reaction was run with CuSO<sub>4</sub>/sodium ascorbate as the catalyst. The reaction stoichiometry was arbitrarily fixed to 1:5 mol% between the estimated azido groups at the CNTs and the acetylene moiety of **3**, respectively. The catalyst amount was more precisely tuned and fixed to 10 mol% with respect to the reactive terminal alkyne. Finally, the functionalised material (**14**) underwent successive sonication/centrifugation/washing cycles and filtration through a 0.2 μm pore inorganic membrane before being dried under vacuum to give a constant weight. Afterwards, selective disulfide bond chemical cleavage was performed on **14**, upon treatment with DTT in a 25:75 mixture of DMF/PBS (Scheme 4). The reaction was followed spectroscopically by monitoring the evolution of **9** (and **5**, see below) until completion after 1 h at 50 °C. Unlike the homogeneous process, disulfide cleavage in **14** does not proceed quantitatively at room temperature, even after several hours, although gentle heating of the reaction mixture rapidly drives the process to completion (Scheme 4; **14**→**15**). Similarly to disulfide cleavage, CNT conjugation with natural L-amino acid **10** containing a sulfhydryl moiety (selected as a HS-terminating residue of a model protein chain) is achieved upon reaction under almost identical conditions (Scheme 4; **14**→**16**). The reaction course was again followed spectroscopically, on the basis of dye evolution (**5**, **9**). In a typical procedure, the crude mixture containing either  $f_{SH}$ -SWCNTs

(**15**) or  $f_{SSCyst}$ -SWCNTs (**16**) was centrifuged to remove the suspended solid material, and the reaction course was monitored by sampling 1 mL of the clear supernatant and analysing it by UV/Vis spectroscopy. Figure 2 shows the UV/Vis measurements on the solutions before (grey, dashed lines) and after treatment with a thiol (red, solid lines for treatment with DTT and **10**). In the case of DTT, the red line highlights the appearance of two

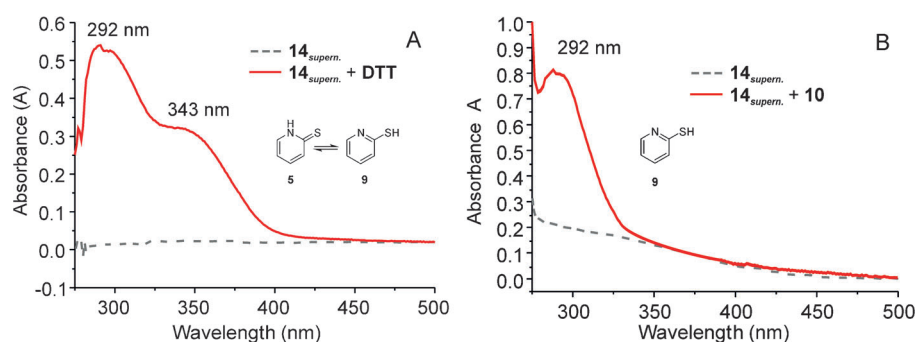


**Figure 2.** UV/Vis measurements on the reaction supernatant before and after treatment of **14** with a selected thiol: A) DTT, 20-fold excess, or B) **10**, 5-fold excess.

absorbance bands at  $\lambda = 292$  and 343 nm (Figure 2A), owing to the coexistence of the two tautomeric forms of the pyridine-based dye in solution (**5** and **9**); the relative intensities measured account for the complete cleavage/conjugation processes (see the Experimental Section). As expected for aprotic reaction media, only **9** results from the treatment of **14** with **10** (Figure 2B).

The functionalised nanomaterials **14** and **16** have been characterised through different chemical (elemental analysis), spectroscopic/spectrometric (FTIR, thermogravimetric analysis (TGA–MS)) and morphological (TEM) techniques. First evidence of the CuAAC reaction occurrence to give **14** was qualitatively achieved by comparing the TGA–MS profile of **14** with that of the starting material **13**. For the sake of consistency, all comparative measurements were performed on a starting material

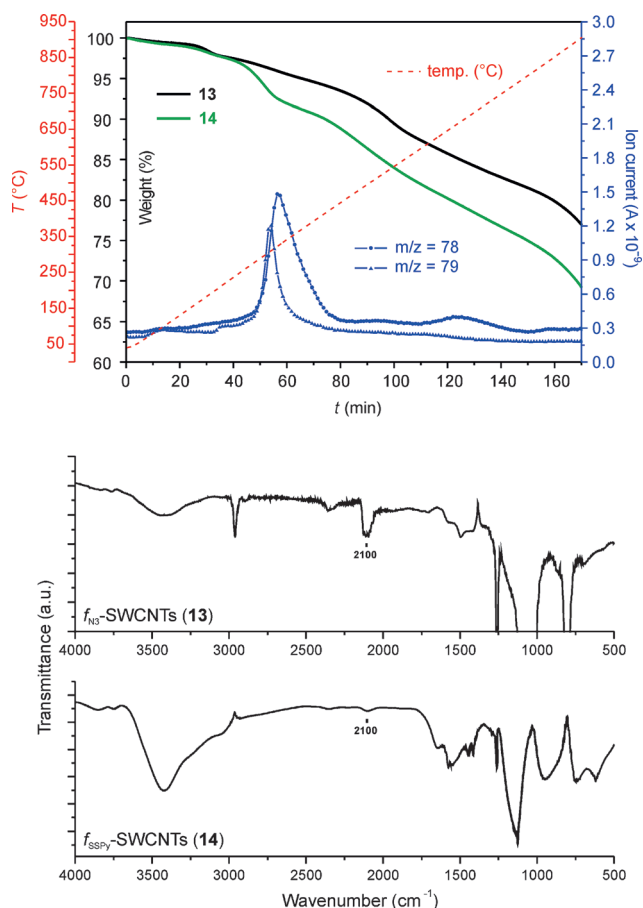


**Figure 3.** Top: TGA profiles ( $N_2$  atm,  $50\text{ mL min}^{-1}$ ) of **13** and **14** associated with the MS analysis of volatile compounds ( $m/z$ : 78 and 79) from **14**. Bottom: FTIR spectra of **13** and **14**.

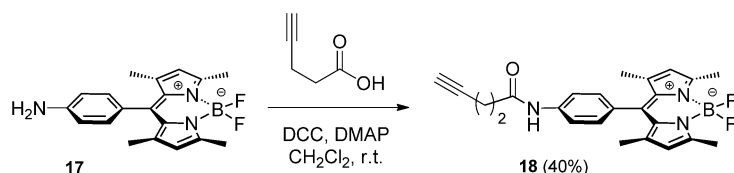
(**13**) that was exposed to identical reaction conditions and reagents, except for the use of the copper catalyst ("blank sample"). As shown in Figure 3, top, a weight loss of 13.7% was measured on sample **14** in the  $200\text{--}450\text{ }^\circ\text{C}$  temperature range (calculated as the weight difference between the TGA profiles of **13** and **14**). Most importantly, analysis of the volatile compounds in the same temperature range revealed the appearance of two distinctive fragmentation signals, which were typical of pyridine units ( $m/z$ : 79  $[M]^+$ , 78  $[M-1]^+$ ) and exclusively present in sample **14**. At higher temperatures ( $>450\text{ }^\circ\text{C}$ ), only gradual, comparable and indistinctive weight losses were observed for the two materials.

The nitrogen and carbon quantitative elemental analysis ( $f_{N_3}$ -SWCNTs (**13**; blank sample): N 2.67, C 87.71, S 0.06;  $f_{SSPy}$ -SWCNTs (**14**): N 3.31, C 77.99, S 2.70) also provided evidence of functionalisation.<sup>[21]</sup> From the TGA measurements, it can be inferred that about 0.543 mmol of  $-C_6H_4-(C_2HN_3)-CH_2NHCO(CH_2)_2S_2(C_6H_5N)$  pendant arm per gram of **13** were consumed in the  $200\text{--}450\text{ }^\circ\text{C}$  temperature range.<sup>[22]</sup> This is in good agreement with the functionalisation loading measured from elemental analysis, for which 0.412 and 0.473 mmol were

calculated from the sulfur and nitrogen content, respectively. In addition, the FTIR spectrum of sample **14** clearly shows an almost complete suppression of the relatively intense  $\nu(N_3)$  asymmetric stretching close to  $\tilde{\nu}=2100\text{ cm}^{-1}$  (Figure 3, bottom), which accounts for an only minor residual amount of  $-C_6H_4-N_3$  groups that are unreactive under the adopted CuAAC conditions.

For the reaction with **10**, qualitative evidence of L-amino acid grafting was provided by a comparison of the TGA profiles of **14** and **16** with the respective MS analysis of volatile compounds. As shown in Figure S1 in the Supporting Information, the TGA profile of **16** does not show any distinctive weight loss in the  $40\text{--}900\text{ }^\circ\text{C}$  temperature range, but only gradual decomposition. If only an extra and indistinct 6.4% weight loss can be measured at the end of the TGA analysis on **16**, the MS analysis of volatile compounds gives more clear evidence of L-cysteine conjugation. Indeed, MS signals owing to the pyridine units ( $m/z$ : 79  $[M]^+$ , 78  $[M-1]^+$ ) are totally suppressed in **16**, whereas two new and distinctive fragmentation signals owing to the thermal decomposition and rearrangement of the *tert*-butoxyl groups of the *N*-BOC-protected moieties ( $m/z$ : 56  $[M]^+$ , 55  $[M-1]^+$  relative to isobutene evolution) clearly increase (Figure S1 in the Supporting Information).

Similarly, CNT hetero-decoration is performed by treating **13** with a controlled mixture of selected alkyne end-capped molecules. At odds with our previous research, the final goal of this study goes beyond the production of complex carbon nanostructures with broad chemical diversity, and aims to provide functional nanomaterials as easily and cleanly post-derivatisable macromolecular fluorescent probes. With this aim, alkyne derivative **18** of the fluorescent BODIPy scaffold was conveniently prepared in good yield and in a single reaction step from the BODIPy aniline<sup>[23]</sup> **17** and 4-pentynoic acid under classical amidation conditions (Scheme 5).

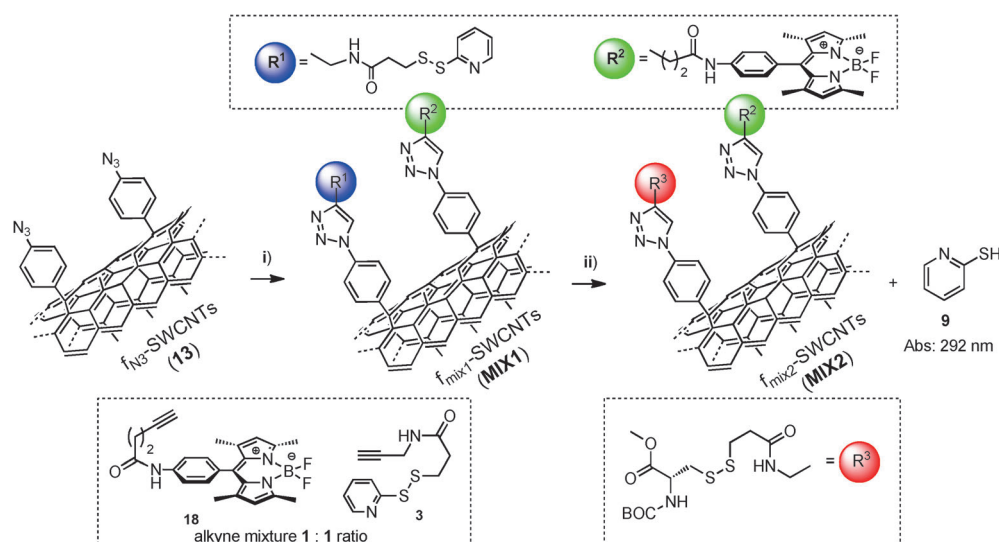


**Scheme 5.** Synthesis of an alkyne-terminated BODIPy scaffold from the BODIPy aniline **17**. DMAP = 4-dimethylaminopyridine.

Similarly to related BODIPy derivatives,<sup>[23d]</sup> the amidation reaction does not significantly affect the fluorescent properties of the BODIPy core (Figure S2 in the Supporting Information).<sup>[23a]</sup>

The chemical approach to CNT hetero-decoration through CuAAC chemistry consists of the use of an equimolar mixture of the two acetylene end-capped molecules **18** and **3**; (Scheme 6) the total amount (mmol) of acetylene reactants is kept equal to that used in the homo-decoration experiment.<sup>[24]</sup>

In a typical procedure, compounds **18**, **3** and **13** were reacted in degassed DMF at  $85\text{ }^\circ\text{C}$  for 2 days in the presence of a catalytic amount (10 mol% with respect to the alkynes content)



**Scheme 6.** Hetero-decoration through the CuAAC reaction between arylazido-functionalised **13** and a 1:1 mixture of the alkyne-terminated spacer **3** and BODIPy fluorescent derivative **18**. i) **13** (0.020 g), **18/3** (1:1; 0.17 mmol overall), Cu[P(OEt)<sub>3</sub>] (0.017 mmol), DMF, 85 °C, 48 h. Post-derivatisation of the  $f_{\text{MIX1}}$ -SWCNTs through conjugation with a HS-terminating amino acid residue ( $f_{\text{MIX1}}$ -SWCNTs  $\rightarrow$   $f_{\text{MIX2}}$ -SWCNTs). ii) **10** (0.05 mmol), DMF, 50 °C, 1 h.

of Cu[P(OEt)<sub>3</sub>]. Successive and multiple sonication/centrifugation/washing cycles were accomplished on the hetero-functionalised material **MIX1** to remove unreacted alkynes and physisorbed reagents. Filtration/washing through a 0.2  $\mu\text{m}$  pore inorganic membrane was used to recover the sample and the solid was finally dried under vacuum to give a constant weight.

Afterwards, the **MIX1** material underwent a reaction with **10** under gentle heating, and the process (**MIX1** vs. **MIX2**) was followed spectroscopically on the basis of the formation of by-product **9**. The UV/Vis measurements on the reaction solutions before (grey, dashed lines in Figure 4) and after treatment with **10** (blue, solid line) clearly show the appearance of an absorbance at  $\lambda = 292 \text{ nm}$  (Figure 4, left), owing to the release of the pyridine-based dye **9**. By assuming complete covalent grafting of **10** to the nanotubes through the disulfide bridge (see below), the measured absorbance intensity accounts for the functionalisation loading of **3**. The fluorescence spectra (Figure 4, right) recorded upon excitation of the solid samples at  $\lambda = 488 \text{ nm}$ , before (**MIX1**) and after (**MIX2**) addition of **10**, are consistent with samples that maintain almost unchanged fluorescence properties.

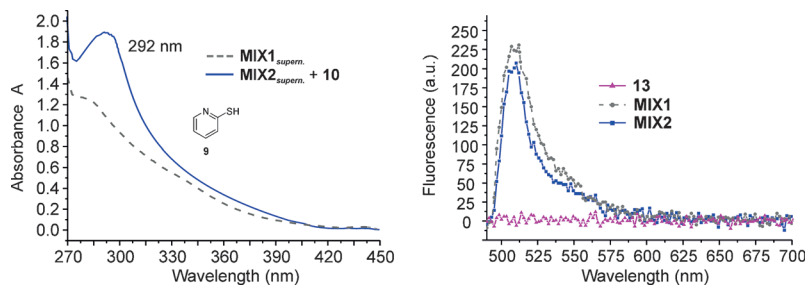


**Figure 4.** Left: UV/Vis measurements on the reaction supernatant before (dashed grey line) and after (blue solid line) treatment of **MIX1** with **10**. Right: Fluorescence spectra of **MIX1** and **MIX2**.

For the sake of completeness, the effect of covalent grafting of the dye to the surface of the SWCNTs on the fluorescence properties is briefly discussed. A remarkable decrease in the dye fluorescence signal is commonly observed on nanotube-dye hybrids, for which the support itself (CNT) and the presence of metal impurities (coming from the CNT synthesis) can dramatically compromise (quench) the fluorescence dye emission.<sup>[25]</sup> As shown in Figure S3 in the Supporting Information, in the case of **MIX1**, the fluorescence emission is reduced up to 80% relative to that recorded for free dye **18** (assuming equal dye concentrations in **MIX1** and **18**).

TGA-MS analyses and IR spectra of **MIX1** and **MIX2** account for a complete conversion of the azido groups on **13** (Figure 5 and Figure S3 in the Supporting Information). Although only a gradual thermal decomposition takes place on both samples with no distinctive weight losses, the measured weight loss difference and the MS analysis of volatile compounds give clear evidence of the transformations that occur. As shown in Figure S4 in the Supporting Information, a weight loss of 21.3% was measured for **MIX1** in the 40–875 °C temperature range (calculated as the weight difference between the TGA profiles of **13** and **MIX1**). In addition, the analysis of volatile compounds in the 200–450 °C temperature range again shows the appearance of two fragmentation signals owing to pyridine units ( $m/z$ : 79 [ $M$ ]<sup>+</sup>, 78 [ $M-1$ ]<sup>+</sup>) and are ascribed to partial material functionalisation with the spacer **3**. Notably, MS analysis of **MIX2** reveals the complete suppression of the pyridine signals, whereas distinctive fragmentations ascribed to the thermal decomposition/rearrangement of the protecting *tert*-butoxyl groups (isobutene:  $m/z$ : 56 [ $M$ ]<sup>+</sup>, 55 [ $M-1$ ]<sup>+</sup>) can be clearly observed in the narrower 125–275 °C temperature range (Figure 5, top); these results offer clear evidence of ligand exchange at the disulfide bridge between the pyridine-2-thiolate group and the incoming *N*-BOC-L-cysteine methyl ester.

The nitrogen, carbon, and sulfur elemental analysis results (**13** (blank sample): N 3.07, C 84.55, S 0.03; **MIX1**: N 4.73, C 74.98, S 1.82; **MIX2**: N 3.25, C 77.81, S, 0.95) do not offer more than a qualitative outlook on the two successive reaction pathways (**13**  $\rightarrow$  **MIX1**  $\rightarrow$  **MIX2**) with a trend of the carbon, nitrogen, and sulfur ratio lying on the ex-

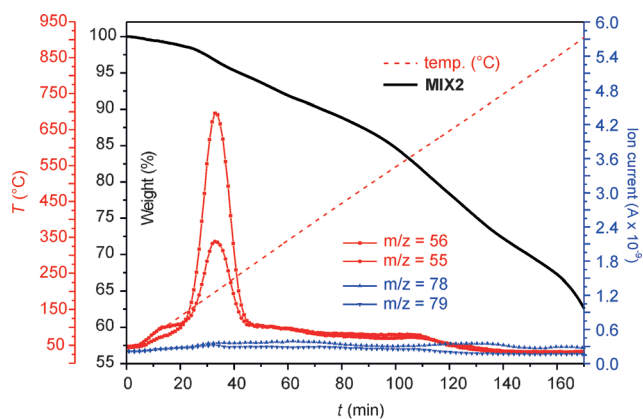


**Figure 5.** Top: TGA profiles ( $N_2$  atm,  $50 \text{ mL min}^{-1}$ ) of **MIX2** associated with the MS analysis of volatile compounds ( $m/z$ : 55 and 56, 78 and 79). Bottom: FTIR spectra of **13**, **MIX1** and **MIX2**.

pected values for a roughly 50:50 **3/18** functionalisation in **MIX1** and the expected ligand exchange in **MIX2**.

A morphological study based on TEM analysis of **13** and **MIX2** unveils a higher degree of CNT aggregation on the multi-decorated sample, with the generation of highly ordered and straight bundles made of tens of SWCNTs (Figure 6A vs. B).

Although any reasonable explanation for this morphological change is merely speculative, a cohesive effect driven by CNT surface modification/decoration with highly conjugated polyaromatic frameworks can be invoked. The fluorescently labelled sample **MIX2** has also been analysed by confocal laser scanning fluorescence microscopy to evaluate the dye distribution at the material surfaces. As shown in Figure 7, the confocal

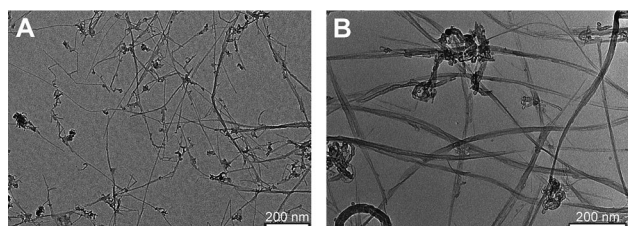


**Figure 6.** TEM images of samples **13** (A) and **MIX2** (B).

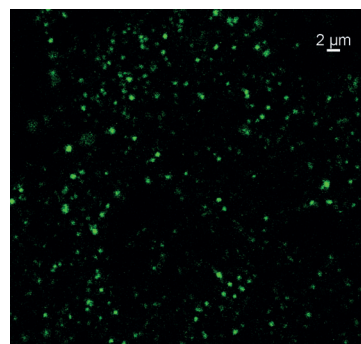


**Figure 7.** Confocal laser scanning fluorescence microscopy of sample **MIX2**: fluorescence image collecting photons in the range  $\lambda = 500\text{--}550 \text{ nm}$ .

image obtained upon material excitation at  $\lambda = 488 \text{ nm}$  reveals a prevailing spot-like distribution of the dye on the CNT bundles. Moreover, Z-stack images recorded along the CNT bundles, clearly show the distribution of the fluorescent spots throughout the material thickness (Figure S5 in the Supporting Information). Such an unexpected distribution adds an additional level of complexity to the comprehension of the undertaken CNT functionalisation and post-derivatisation chemistry. One reasonable explanation for the observed surface molecule distribution arises from the nature of the functionalisation approach employed for the initial CNT decoration with phenylazido moieties. The reductive dissociation of diazonium salts with loss of  $N_2$ <sup>[26]</sup> generates aryl radicals that react with carbon-carbon double bonds along the nanotube wall, according to the Meerwein arylation path.<sup>[27]</sup>

The as-generated  $(Ar)_{n-1}$ -CNT radical species can be rapidly intercepted and trapped by a second aryl radical reagent; thus allowing a close distribution of the chemically grafted functionalities. In addition, the  $sp^2$ -network perturbation owing to the aryl radical attack induces the local generation of high-energy sites (defects), which are potentially suitable for an additional (and proximal) chemical attack. Moreover, the observed spot-like distribution of the BODIPy dye derivative can also originate from a multilayered aryl coating of the CNT surface. Menna and co-workers have recently demonstrated how a simple modulation of the aryldiazonium salt concentration under classical Tour conditions could promote the growth of multilayered structures.<sup>[28]</sup> This process, also named CNT superfunctionalisation, was expected to increase the concentration of the aryl functionalities locally; as a consequence, their subsequent post-derivatisation (click chemistry) would result in spatially confined fixation of the newly introduced functionalities (i.e., the formation of dye “spots” throughout the material).

Fluorescence lifetime measurements on sample **MIX2** revealed the co-existence of two different fluorescence decays. In particular, lifetimes of 4.2 and 0.5 ns (the former strongly dominates) have been measured (Figure S6 in the Supporting Information).<sup>[29]</sup> The shorter lifetime may be due to the close proximity of dyes in a spot, as well as fluorescence quenching effects owing to the CNTs.

## Conclusion

We described the synthesis of a linear hetero-functional cross-linker featuring a cleavable disulfide moiety for the covalent anchoring of a wide range of thiol end-capped (bio)molecules and, through a clickable terminal acetylene group, the CuAAC reaction at the surface of phenylazido-decorated carbon-based nanostructures. The bio-orthogonal character of the click reaction makes it highly desirable for conjugating CNTs and biomolecules.<sup>[12,30]</sup> The adopted methodology generated multifunctional CNT platforms, in which disulfide bond cleavage, operating through sulfhydryl-containing molecules, occurred with the controlled release of a pyridine dye, the concentration of which was proportional to the extent of cleavage or conjugation by an incoming thiol end-capped molecule. As a result, the cleavage/functionalisation scheme provided a useful tool for the chemical linkage of a wide range of thiol-terminating probes to the carbon nanomaterial surface, and precise functionalisation loading was simply assessed by UV/Vis measurements. Controlled CNT hetero-decoration through a one-step CuAAC reaction with an acetylene mixture composed of the bifunctional linker and an acetylene fluorescence dye (BODIPy derivative) was used to impart multifunctionality on the final carbon nanohybrid. This approach generated optically traceable nanocarriers, the conjugation of which with sulfhydryl-containing (bio)molecules was allowed through simple ligand exchange at the disulfide bridge. Most importantly, each functionalisation and post-derivatisation step could be precisely followed by spectroscopic measurements (UV/Vis) of the reaction solutions by monitoring the release of a pyridine dye. A morphological study of the as-prepared hetero-decorated nanohybrids provided interesting insights into the ultimate distribution of the functional groups at the nanomaterial surface, as a consequence of the regiochemical attachment of radical species generated from aryl diazonium intermediates.

## Experimental Section

### General

All reactions were performed under a dry nitrogen atmosphere by using standard Schlenk techniques. Nitrogen (>99.999%; Rivoira) was dried through a CaCl<sub>2</sub> column and deoxygenated with an oxygen sorb cartridge from Messer Griesheim prior to use. Dichloromethane was freshly distilled over CaH<sub>2</sub> prior to use, dry DMF, ortho-dichlorobenzene (oDCB) and triethylamine were purified according to literature procedures<sup>[31]</sup> and stored over 4 Å molecular sieves under a nitrogen atmosphere. Acetonitrile was obtained by means of an MBraun solvent purification system. Pristine SWCNTs (90% C) were purchased from NanoAmor and used without further purification. Phenylazido-decorated SWCNTs (**13**),<sup>[11]</sup> amino- (**17**)<sup>[32]</sup> and azidophenyl BODIPy (**6**)<sup>[33]</sup> compounds were prepared according to literature procedures. Unless otherwise stated, all other chemicals/solvents were purchased from commercial suppliers and used as received without further purification.

Sample sonication was performed by using an Elma S15 Elmasonic sonicator bath (37 kHz), while cooling samples in a water/ice mixture throughout the whole treatment. CNT filtration was accomplished by using polytetrafluoroethylene (PTFE) membranes/filters

(Whatman) with 0.2 μm pore size. All measurements performed on pristine SWCNTs and functionalised materials (*f*-SWCNTs) were conducted on samples that underwent identical washing/sonication/filtration workup procedures.

### Material characterisation and analyses conditions

TGA was performed under a nitrogen atmosphere (50 mL min<sup>-1</sup>) on an EXSTAR thermogravimetric analyser (TG/DTA) Seiko 6200 coupled with a ThermoStar GSD 301T (TGA-MS) for MS analysis of volatile compounds. FTIR spectroscopy was performed on a Perkin-Elmer Spectrum BX FTIR spectrophotometer and CNT samples were prepared by mixing spectroscopic-grade KBr with pristine SWCNTs or *f*-SWCNTs (2–3 wt%) and analysed in the  $\tilde{\nu}$  = 400–4000 cm<sup>-1</sup> range with a resolution of 1 cm<sup>-1</sup>. IR spectra of pristine SWCNTs (2–3 wt%)/KBr was used as a background and directly subtracted from the spectra of the functionalised (*f*-SWCNTs) samples. <sup>1</sup>H and <sup>13</sup>C NMR spectra of all organic products and intermediates were obtained on a Bruker Avance 300 MHz instrument. Chemical shifts are reported in ppm ( $\delta$ ) relative to tetramethylsilane (TMS) and referenced to the chemical shifts of residual solvent resonances. Elemental analysis were performed on a Thermo FlashEA 1112 Series CHNS-O elemental analyser with an accepted tolerance of 0.4 units on C, H, N and S. UV/Vis measurements were performed on a PerkinElmer UV/VIS/NIR Lambda 19 spectrometer. ESI-MS was acquired on a LCQ-Fleet Thermo Scientific ion trap mass spectrometer by using diluted sample solutions (10<sup>-5</sup> M) in MeOH. Fluorescence measurements were performed on a laboratory setup by using, for excitation, a Nichia NDS1113E laser diode with emission at  $\lambda$  = 486 nm, filtered by means of an interference band pass optical filter Andover 488FS10 (central wavelength:  $\lambda$  = 488 nm; bandwidth: 10 nm full-width at half-maximum (FWHM)). The emitted fluorescence was collected by means of a multimode optical fibre coupled with a collimating GRIN lens, filtered by means of an interference long-pass optical filter Semrock BLP01-488R-25 (cut-on wavelength:  $\lambda$  = 500 nm) to block excitation scattered light, and detected on a spectrometer Andor Shamrock 303i instrument. Confocal fluorescence imaging was performed on an inverted Nikon A1 laser scanning confocal microscope equipped with a continuous wave (CW) argon ion laser for excitation at  $\lambda$  = 457, 488 and 514 nm (Melles Griot, 40 mW), and a diode laser for excitation at  $\lambda$  = 485 nm (LDH-D-C-405 of Picoquant GmbH Berlin, Germany) operating both in continuous mode (50 mW) and pulsed at 40 MHz (1.0 mW average power for pulse FWHM of 120 ps). Confocal fluorescence imaging was performed on the samples at room temperature. The images were collected by using a Nikon PLAN APO VC 20× or Nikon PLAN APO VC 60× oil immersion objective with NA 0.95 and 1.40, respectively. Images of 512×512 pixels were acquired and pixel dimension of the *xy* plane fell in the range 0.1–0.4 μm. The hexagonal pinhole dimension was set to 1.0 a.u., which corresponded to 38 μm and an optical thickness of 440 nm. Two dichroic mirrors reflecting either  $\lambda$  = 405 and 488 nm or  $\lambda$  = 405, 488, 541 and 640 nm were used. Bandpass filters in front of the photomultiplier tube (PMT)-selected fluorescence in the ranges  $\lambda$  = 500–550 and 570–620 nm. Spectral imaging was achieved with a Nikon 32-PMT array detector with resolution varying from 6 to 10 nm per channel. For fluorescence lifetime imaging, a time-correlated single photon counting (TCSPC) system of Picoquant GmbH, Berlin, was used with excitation at  $\lambda$  = 485 nm. Photons were detected in time tagged time resolved (TTTR) mode with two single-photon avalanche diodes manufactured by Micro Photon Devices (MPD), Bolzano, Italy. Fluorescence was filtered with the opportune fluorescence SEMROCK bandpass filters  $\lambda$  = 520/40, and 585/40 nm.

A PicoHarp 300 photon processor completed the TCSPC system. SymPhoTime v. 5.1 analysis software was used for image processing and lifetime fitting. A tail fit with multi-exponential functions was performed to analyse fluorescence decays of selected regions of interest (ROI). The system allowed measurement of fluorescence lifetimes from 300 ps to several nanoseconds.

### Synthesis of 3-(tritylthio)propionic acid (1)

The carboxylic acid derivative **1** was prepared according to a literature procedure<sup>[14]</sup> and the final product was isolated in 90% yield as analytically pure white crystals. <sup>1</sup>H NMR (300 MHz, CDCl<sub>3</sub>, selected data): δ = 2.25 (t, <sup>3</sup>J = 7.2 Hz, 2H), 2.48 (t, <sup>3</sup>J = 7.2 Hz, 2H), 7.23–7.33 (9H), 7.33–7.45 ppm (6H); elemental analysis calcd (%) for C<sub>22</sub>H<sub>20</sub>O<sub>2</sub>S: C 75.83, H 5.78, S 9.20; found: C 76.09, H 5.91, S 9.05. For additional characterisation data, see ref. [14].

### Synthesis of *N*-(prop-2-ynyl)-3-(tritylthio)propanamide (2)

HOBt (2.56 g, 18.9 mmol) and DCC (3.90 g, 18.9 mmol) were added in sequence to a solution of **1** (6 g, 17.2 mmol) in dry and degassed DMF (120 mL), and the resulting mixture was maintained under stirring at room temperature for 3 h until completion of the reaction. The reaction course was followed by TLC (eluent: petroleum ether/AcOEt = 60/40) to monitor the progressive disappearance of starting acid **1**. Et<sub>3</sub>N (2.88 mL, 20.6 mmol) and propargylamine (1.4 mL, 20.6 mmol) were added and the resulting mixture was stirred at room temperature for 24 h. The reaction was quenched by adding a dilute solution of HCl (0.05 M, 120 mL) followed by CH<sub>2</sub>Cl<sub>2</sub> (120 mL). The organic mixture was then extracted and the aqueous phase was treated with brine (120 mL). The aqueous mother liquors were then extracted three times with CH<sub>2</sub>Cl<sub>2</sub> (3 × 90 mL). The collected organic phases were dried over Na<sub>2</sub>SO<sub>4</sub> and evaporated to dryness under reduced pressure. The crude semi-solid material was purified by flash chromatography (SiO<sub>2</sub>, petroleum ether: AcOEt = 60:40) to give **2** as a white solid (91% yield). <sup>1</sup>H NMR (300 MHz, CDCl<sub>3</sub>): δ = 2.03 (t, <sup>3</sup>J = 7.3 Hz, 2H), 2.23 (t, <sup>3</sup>J = 2.4 Hz, 1H), 2.53 (t, <sup>3</sup>J = 7.3 Hz, 2H), 3.99 (m, 2H), 7.23–7.26 (10H), 7.33–7.46 ppm (5H); <sup>13</sup>C{<sup>1</sup>H} NMR (75 MHz, CDCl<sub>3</sub>): δ = 27.5, 29.2, 35.4, 66.9, 71.7, 79.4, 126.8, 128.0, 129.6, 144.6, 170.6 ppm; IR (KBr):  $\tilde{\nu}$  = 1636.4 cm<sup>-1</sup> (C=O); elemental analysis calcd (%) for C<sub>25</sub>H<sub>23</sub>NOS: C 77.89, H 6.01, N 3.63, S 8.32; found: C 78.01, H 5.91, N 3.68, S 8.35.

### Synthesis of *N*-(prop-2-ynyl)-3-(pyridin-2-yl)disulfanylpropanamide (3)

1,2-Di(pyridin-2-yl)disulfane (10.3 g, 46.8 mmol) and Et<sub>3</sub>SiH (2.75 mL, 17.2 mmol) were added in sequence to a solution of **2** (6 g, 15.6 mmol) in dry and degassed CH<sub>2</sub>Cl<sub>2</sub> (140 mL). TFA (35 mL) was added dropwise to the resulting mixture, and the system was maintained under stirring at RT for 4 h. The mixture was concentrated to a reduced volume and treated with AcOEt/Et<sub>3</sub>N (1:1; 550 mL). The solution was stirred at room temperature overnight before being diluted with water (550 mL). The resulting phases were separated and the aqueous liquor was extracted three times with AcOEt (3 × 500 mL). The collected organic layers were dried over Na<sub>2</sub>SO<sub>4</sub> and the solvent was removed under reduced pressure. The crude product was purified by flash chromatography (SiO<sub>2</sub>, AcOEt/petroleum ether 80:20) to give **3** as a pale yellow oil (62% yield). <sup>1</sup>H NMR (300 MHz, CDCl<sub>3</sub>): δ = 2.26 (t, <sup>4</sup>J = 2.6 Hz, 1H), 2.64 (t, <sup>3</sup>J = 6.7 Hz, 2H), 3.10 (t, <sup>3</sup>J = 6.7 Hz, 2H), 4.10 (m, 2H), 7.17 (1H),

7.62 (1H), 7.69 (1H), 8.56 ppm (1H); <sup>13</sup>C{<sup>1</sup>H} NMR (75 MHz, CDCl<sub>3</sub>): δ = 29.2, 35.1, 35.5, 71.6, 79.8, 120.7, 121.2, 137.5, 149.3, 159.2, 170.7 ppm; IR (KBr):  $\tilde{\nu}$  = 1647.6 cm<sup>-1</sup> (C=O); ESI-MS: *m/z*: 275 [M + Na]<sup>+</sup>; elemental analysis calcd (%) for C<sub>11</sub>H<sub>12</sub>N<sub>2</sub>O<sub>5</sub>: C 52.35, H 4.79, N 11.10, S 25.41; found: C 52.41, H 4.65, N 10.77, S 25.07.

### Synthesis of the alkyne-BODIPy derivative 18

4-Pentynoic acid (0.076 g, 0.79 mmol) in CH<sub>2</sub>Cl<sub>2</sub> (5 mL) was added to a solution of DCC (0.254 g, 1.23 mmol) in CH<sub>2</sub>Cl<sub>2</sub> (5 mL), followed by the addition of **17** (0.268 g, 0.79 mmol) in CH<sub>2</sub>Cl<sub>2</sub> (4 mL). Anhydrous DMAP (0.010 g, 0.079 mmol) was then added and the resulting solution was stirred under nitrogen for 24 h at RT. The reaction mixture was then diluted with CH<sub>2</sub>Cl<sub>2</sub>, washed in sequence with water, a 0.5 M solution of HCl (2 × 40 mL), a saturated solution of NaHCO<sub>3</sub> (2 × 40 mL) and brine. After drying over anhydrous Na<sub>2</sub>SO<sub>4</sub>, the solvent was evaporated and the crude product was purified by flash chromatography on silica gel, eluting first with EtOAc/hexane (1:3) and then with EtOAc/hexane (1:2) to afford **18** as an orange gummy solid (75% yield). <sup>1</sup>H NMR (300 MHz, CDCl<sub>3</sub>): δ = 1.41 (s, 6H), 2.54 (s, 6H), 2.63 (m, 4H), 5.97 (s, 2H), 7.23 (2H), 7.69 (2H), 7.83 ppm (1H); <sup>13</sup>C{<sup>1</sup>H} NMR (75 MHz, CDCl<sub>3</sub>): δ = 14.6, 24.9, 25.5, 33.9, 36.3, 49.3, 53.4, 69.8, 82.8, 120.0, 121.7, 128.7, 130.6, 131.6, 138.7, 141.2, 143.1, 155.4, 169.4 ppm; IR (KBr):  $\tilde{\nu}$  = 1658.6 cm<sup>-1</sup> (C=O); elemental analysis calcd (%) for C<sub>25</sub>H<sub>29</sub>BF<sub>2</sub>N<sub>3</sub>O: N 9.63, C 68.82, H 6.70; found: N 9.76, C 68.65, H 6.91.

### Homogeneous CuAAC reaction on **3** with the azido-BODYPy derivative **6**

Compound **3** (0.55 mmol), CuSO<sub>4</sub> (0.02 mmol) and sodium ascorbate (0.04 mmol) were added in sequence to a solution of **6** in dry and degassed DMF (2 mL). The mixture was stirred for 24 h at 50 °C under a nitrogen atmosphere. Distilled water (20 mL) was added and the mixture was extracted with AcOEt (3 × 15 mL). The collected organic phases were washed twice with water (2 × 30 mL) before being dried over Na<sub>2</sub>SO<sub>4</sub> and concentrated under reduced pressure. The crude material was purified by flash chromatography over silica gel (eluent: AcOEt/petroleum ether: 80/20) to afford **7** as dark-red crystals (45% yield (93% yield if we consider the recovery of azido reagent **6** during chromatographic purification)). The reaction was also performed by using CuI[P(OEt)<sub>3</sub>] as an alternative soluble CuAAC catalyst under identical experimental conditions, without any appreciable improvement in yield. <sup>1</sup>H NMR (300 MHz, CDCl<sub>3</sub>): δ = 1.44 (s, 6H), 2.58 (s, 6H), 2.66 (t, <sup>3</sup>J = 6.7 Hz, 2H), 3.11 (t, <sup>3</sup>J = 6.7 Hz, 2H), 4.66 (d, <sup>3</sup>J = 5.8 Hz, 2H), 6.00 (s, 2H), 7.13 (1H), 7.46 (2H), 7.55–7.65 (3H), 7.90 (2H), 8.15 (1H), 8.51 ppm (1H); <sup>13</sup>C{<sup>1</sup>H} NMR (75 MHz, CDCl<sub>3</sub>): δ = 14.5, 14.7, 34.7, 35.6, 120.6, 120.9, 121.3, 121.7, 130.0, 131.3, 135.5, 137.1, 137.4, 139.5, 142.9, 146.2, 149.9, 156.2, 159.1, 171.1 ppm; IR (KBr):  $\tilde{\nu}$  = 1647.6 cm<sup>-1</sup> (C=O); elemental analysis calcd (%) for C<sub>30</sub>H<sub>30</sub>BF<sub>2</sub>N<sub>7</sub>OS<sub>2</sub>: C 58.35, H 4.90, N 15.88, S 10.38; found: C 58.41, H 4.65, N 15.77, S 10.07.

### General procedure for the homo- and hetero-derivatisation of phenylazido-decorated SWCNTs through the CuAAC reaction

The CuAAC protocol used for the homo- and hetero-derivatisation of **13** to give **14**, **MIX1** and **MIX2** hybrids followed that already described by some of us.<sup>[11]</sup> In a typical procedure, *f*<sub>N3</sub>-SWCNTs (20 mg) were suspended in dry and degassed DMF (3 mL) and sonicated for 15 min. The resulting suspension was treated in se-

quence with **3** (0.17 mmol) or an equimolar mixture of **3/18** (0.17 mmol overall), and CuI[P(OEt)<sub>3</sub>] (6 mg, 0.017 mmol). The mixture was then sonicated for 30 min and heated at 85 °C, while being stirred under a nitrogen atmosphere for 48 h. After cooling to room temperature, the suspension was diluted with ethyl acetate, sonicated for additional 10 min and centrifuged to recover the solid residue by simple decantation. The solid was washed and sonicated three times with AcOEt and CH<sub>2</sub>Cl<sub>2</sub> (1 × 10 mL AcOEt, 2 × 10 mL CH<sub>2</sub>Cl<sub>2</sub>) and the supernatant solution was removed after centrifugation. Finally, the solid residue was suspended in CH<sub>2</sub>Cl<sub>2</sub> (15 mL), sonicated for 10 min and filtered through inorganic membranes/filters (Whatman) with 0.2 μm pore size before being dried under vacuum at 50 °C to give constant weight.

#### General procedure for the disulfide cleavage of **3**, **7** and SWCNT composite **14** by a model dithiol and subsequent monitoring of the reaction course by UV/Vis measurements

In a typical procedure, disulfide **3** (0.5–1 mg) was accurately weighted by using a Sartorius 4503 microbalance ( $d=0.001$  mg) and dissolved in a mixture of DMF/PBS (2 mL; 25:75; pH 7.2). The solution was divided into two portions: the first was directly analysed by UV/Vis spectroscopy ("blank" sample), whereas the second was treated with a 20-fold excess of a solution of model thiol (DTT). After 15 min at room temperature, the solution was analysed by UV/Vis spectroscopy under the same conditions as those used for the blank sample. The difference, in terms of absorbance values, measured between the two samples at  $\lambda=343$  nm was correlated with the amount of **5** released from the spacer by using the Lambert–Beer equation [Eq. (1)]:

$$C \text{ (mol L}^{-1}\text{)} = (A_{\text{sample}} - A_{\text{blank}}) / (\epsilon \text{ (M}^{-1} \text{ cm}^{-1}\text{)} \times b \text{ (cm)}) \quad (1)$$

in which  $\epsilon$  is the molar extinction coefficient of **5** (8080 M<sup>-1</sup> cm<sup>-1</sup>) and  $b$  is the optical path (1 cm).

The same procedure was followed for sample **7**, except TDT was used as a model cleaving agent (for solubility reasons) in pure DMF as the solvent to give **8** and **9**.

An identical procedure to that described for the homogeneous disulfide cleavage of **3** was employed for the SWCNT samples containing the disulfide spacer (samples **14** → **15**), except for keeping, after the addition of DTT, the well-sonicated samples under heating (50 °C) for 1 h to bring the cleavage process to completion. The resulting suspension was centrifuged and the supernatant was analysed by UV/Vis spectroscopy.

#### Covalent grafting of **10** on **3** to give **11**

A solution of **3** (0.02 g, 0.08 mmol) in dry and degassed DMF (1.5 mL) was treated with a solution of **10** (0.025 mL, 0.12 mmol) in DMF (0.5 mL) and the resulting solution was maintained under stirring at RT for 6 h. After cooling to room temperature, the reaction was quenched with distilled water (20 mL) and extracted with CH<sub>2</sub>Cl<sub>2</sub> (3 × 25 mL). The collected organic phases were dried over Na<sub>2</sub>SO<sub>4</sub> and concentrated under reduced pressure. The crude product was purified by flash chromatography (SiO<sub>2</sub>, AcOEt/petroleum ether 50:50) to afford **11** as a colourless oil (62% yield). <sup>1</sup>H NMR (300 MHz, CDCl<sub>3</sub>):  $\delta=1.45$  (s, 9H), 2.22 (s, 1H), 2.61 (m, 2H), 2.93–3.19 (4H), 3.77 (s, 3H), 4.07 (m, 2H), 4.60 (m, 1H), 5.36 (m, 1H), 6.32 ppm (s, 1H); <sup>13</sup>C{<sup>1</sup>H} NMR (75 MHz, CDCl<sub>3</sub>):  $\delta=28.3$ , 29.3, 34.0, 35.9, 41.9, 52.7, 53.2, 71.6, 79.4, 80.5, 155.2, 170.5, 171.2 ppm; IR (KBr):  $\tilde{\nu}=1744.2$  (MeO–C=O), 1708.3 (tBuO–C=O), 1653.1 cm<sup>-1</sup> (NH–

C=O); elemental analysis calcd (%) for C<sub>15</sub>H<sub>24</sub>N<sub>2</sub>O<sub>5</sub>S<sub>2</sub>: C 47.85, H 6.43, N 7.44, S 17.03; found: C 47.41, H 6.55, N 7.77, S 17.07.

#### Covalent grafting of **10** on **7** to give **12**

A solution of **7** (0.035 g, 0.06 mmol) in dry and degassed DMF (1.5 mL) was treated with a solution of **10** (0.02 mL, 0.08 mmol) in DMF (0.5 mL) and the resulting mixture was maintained under stirring at RT for 6 h. The reaction was quenched with distilled water (20 mL) and extracted with AcOEt (3 × 25 mL). The collected organic phases were dried over Na<sub>2</sub>SO<sub>4</sub> and concentrated at reduced pressure. The crude product was purified by flash chromatography (SiO<sub>2</sub>, AcOEt/petroleum ether 80:20) to give **12** as red crystals (39% yield). <sup>1</sup>H NMR (300 MHz, CDCl<sub>3</sub>):  $\delta=1.44$  (15H), 2.57 (s, 6H), 2.65 (m, 2H), 3.00–3.14 (4H), 3.77 (s, 3H), 4.62 (3H), 5.36 (1H), 6.01 (2H), 6.67 (1H), 7.49 (2H), 7.93 (2H), 8.15 ppm (1H); <sup>13</sup>C{<sup>1</sup>H} NMR (75 MHz, CDCl<sub>3</sub>, selected data):  $\delta=14.1$ , 28.3, 29.4, 29.7, 30.9, 31.9, 52.7, 53.2, 121.8, 122.8, 129.8, 169.8 ppm; IR (KBr):  $\tilde{\nu}=1749.1$  (v), 1711.1 (v), 1649.1 (v), 1552.2 cm<sup>-1</sup> (δ); elemental analysis calcd (%) for C<sub>34</sub>H<sub>42</sub>BF<sub>2</sub>N<sub>2</sub>O<sub>5</sub>S<sub>2</sub>: C 55.06, H 5.71, N 13.22, S 8.65; found: C 54.81, H 5.65, N 13.37, S 8.27.

#### Covalent grafting of **10** on **14** to give $f_{\text{SSPy}}$ -SWCNTs (**16**)

The  $f_{\text{SSPy}}$ -SWCNTs (20 mg) were suspended in dry and degassed DMF (1.5 mL) and sonicated for 15 min. A solution of **10** (0.010 mL, 0.05 mmol) in DMF (0.5 mL) was added in sequence and the resulting suspension was sonicated for 10 min before being stirred at 50 °C for 1 h. After cooling the mixture to room temperature, AcOEt (10 mL) was added and the suspension was sonicated for 10 min. The solid residue was separated from the mother liquor by centrifugation and submitted to the following workup procedure. The recovered solid residue underwent three successive washing/sonicating cycles (2 × AcOEt, 1 × CH<sub>2</sub>Cl<sub>2</sub>), each time recovering the solid compound by centrifugation. The solid residue was then suspended in dichloromethane, sonicated for an additional 10 min and filtered through a 0.2 μm filter (Whatman) before being dried under vacuum at 50 °C to give a constant weight.

#### Acknowledgements

We thank the "FREECATS" (Doped carbon nanostructures as metal-free catalysts—FP7, NMP-2011-2.2-4) project for financial support of this study. The "NanoMAX-Encoder" project (Engineering Nanostructures for Cellular imaging and for intracellular delivery of Optically active Drugs for cardiac hypERTrophy) is also acknowledged. Finally A.B., S.C. and G.G. also thank the FIRB-(MIUR) Teranostica project (Approcci nanotecnologici per la teranostica dei tumori RBAP11ETKA\_002 and Dr. J. Parlanti for his contribution to this work).

**Keywords:** carbon · click chemistry · drug delivery · nanotubes · synthesis design

- [1] a) A. Krüger in *Carbon Materials and Nanotechnology* (Ed.: A. Krüger), Wiley-VCH, Weinheim, 2010, p. 490; b) V. Georgakilas, M. Otyepka, A.B. Bourlino, V. Chandra, N. Kim, P. Hobza, R. Zboril, *Chem. Rev.* 2012, 112, 6156–6214; c) D. M. Guldi, N. Martín in *Carbon Nanotubes and Related Structures: Synthesis Characterization, Functionalization, and Applications* (Eds.: D. M. Guldi, N. Martín), Wiley-VCH, Weinheim, 2010, p. 562.

- [2] a) D. Tasis, N. Tagmatarchis, A. Bianco, M. Prato, *Chem. Rev.* **2006**, *106*, 1105–1136; b) P. Singh, S. Campidelli, S. Giordani, D. Bonifazi, A. Bianco, M. Prato, *Chem. Soc. Rev.* **2009**, *38*, 2214–2230; c) V. Sgobba, D. M. Guldi, *Chem. Soc. Rev.* **2009**, *38*, 165–184; d) K. Dirian, M. Angeles Herranz, G. Katsukis, J. Malig, L. Rodríguez-Perez, C. Romero-Nieto, V. Strauss, N. Martin, D. M. Guldi, *Chem. Sci.* **2013**, *4*, 4335–4353.
- [3] a) T. Kashiwagi, E. Grulke, J. Hilding, R. Harris, W. Awad, J. Douglas, *Macromol. Rapid Commun.* **2002**, *23*, 761–765; b) C. F. Kuan, W. J. Chen, Y. L. Li, C. H. Chen, H. C. Kuan, C. L. Chiang, *J. Phys. Chem. Solids* **2010**, *71*, 539–543; c) M. T. Byrne, Y. K. Gun'ko, *Adv. Mater.* **2010**, *22*, 1672–1688; d) S. H. Park, P. R. Bandaru, *Polymer* **2010**, *51*, 5071–5077; e) N. G. Sahoo, S. Rana, J. W. Cho, L. Li, S. H. Chan, *Prog. Polym. Sci.* **2010**, *35*, 837–867.
- [4] a) Z. Liu, K. Chen, C. Davis, S. Sherlock, Q. Cao, X. Chen, H. Dai, *Cancer Res.* **2008**, *68*, 6652–6660; b) Z. Liu, S. Tabakman, K. Welscher, H. Dai, *Nano Res.* **2009**, *2*, 85–120; c) M. Prato, K. Kostarelos, A. Bianco, *Acc. Chem. Res.* **2008**, *41*, 60–68.
- [5] a) Z. Liu, A. C. Fan, K. Rakhra, S. Sherlock, A. Goodwin, X. Chen, Q. Yang, D. W. Felsler, H. Dai, *Angew. Chem. Int. Ed.* **2009**, *48*, 7668–7672; *Angew. Chem.* **2009**, *121*, 7804–7808; b) K. Kostarelos, A. Bianco, M. Prato, *Nat. Nanotechnol.* **2009**, *4*, 627–633; c) A. Ruggiero, C. H. Villa, J. P. Holland, S. R. Sprinkle, C. May, J. S. Lewis, D. A. Scheinberg, M. R. McDevitt, *Int. J. Nanomed.* **2010**, *5*, 783–802.
- [6] a) G. Tuci, C. Zafferoni, P. D'Ambrosio, S. Caporali, M. Ceppatelli, A. Rossin, T. Tsoufis, M. Innocenti, G. Giambastiani, *ACS Catal.* **2013**, *3*, 2108–2111; b) G. Tuci, C. Zafferoni, A. Rossin, A. Milella, L. Luconi, M. Innocenti, L. Truong Phuoc, C. Duong-Viet, C. Pham-Huu, G. Giambastiani, *Chem. Mater.* **2014**, *26*, 3460–3470.
- [7] a) N. Karousis, N. Tagmatarchis, D. Tasis, *Chem. Rev.* **2010**, *110*, 5366–5397; b) A. Hirschi, O. Vostrowsky, *Top. Curr. Chem.* **2005**, *245*, 193–237.
- [8] a) C. Samori, H. Ali-Boucetta, R. Sainz, C. Guo, F. M. Toma, C. Fabbro, T. da Ros, M. Prato, K. Kostarelos, A. Bianco, *Chem. Commun.* **2010**, *46*, 1494–1496; b) J. Chen, S. Chen, X. Zhao, L. V. Kuznetsova, S. S. Wong, I. Ojima, *J. Am. Chem. Soc.* **2008**, *130*, 16778–16779.
- [9] N. Wong Shi Kam, Z. Liu, H. Dai, *J. Am. Chem. Soc.* **2005**, *127*, 12492–12493.
- [10] Y.-Z. You, C.-Y. Hong, C.-Y. Pan, *J. Phys. Chem. C* **2007**, *111*, 16161–16166.
- [11] G. Tuci, C. Vinattieri, L. Luconi, M. Ceppatelli, S. Cicchi, A. Brandi, J. Filipi, M. Melucci, G. Giambastiani, *Chem. Eur. J.* **2012**, *18*, 8454–8463.
- [12] J. M. Baskin, C. R. Bertozzi, *QSAR Comb. Sci.* **2007**, *26*, 1211–1219.
- [13] For a conceptually similar approach to the homo- and hetero-decoration of MOF materials see also: G. Tuci, A. Rossin, X. Xu, M. Ranocchiaro, J. A. van Bokhoven, L. Luconi, I. Manet, M. Melucci, G. Giambastiani, *Chem. Mater.* **2013**, *25*, 2297–2308.
- [14] E. L. Ruggles, P. B. Dekker, R. J. Hondal, *Tetrahedron* **2009**, *65*, 1257–1267.
- [15] D. A. Pearson, M. Blanchette, M. L. Baker, C. A. Guindon, *Tetrahedron Lett.* **1989**, *30*, 2739–2742.
- [16] Y. Lin, A. Favre-Re'guillon, S. Pellet-Rostainga, M. Lemaire, *Tetrahedron Lett.* **2007**, *48*, 3463–3466.
- [17] J. C. Kaila, A. B. Baraiya, A. N. Pandya, H. B. Jalani, K. K. Vasu, V. Sudarsanam, *Tetrahedron Lett.* **2009**, *50*, 3955–3958.
- [18] P. A. Wender, E. A. Goun, L. R. Jones, US2010/0255499A1, **2010**.
- [19] The variation of the intensity measured in Figure 1B falls within the repeatability error of the fluorescence measurement setup.
- [20] a) P. Beak, *Acc. Chem. Res.* **1977**, *10*, 186–192; b) S. Stoyanova, I. Petkov, L. Antonov, T. Stoyanova, P. Karagiannidis, P. Aslanidis, *Can. J. Chem.* **1990**, *68*, 1482–1489.
- [21] Elemental analysis provides an overestimated functionalisation loading that is within the same order of magnitude as that calculated from the TGA profile. The nitrogen, carbon and sulfur contents were calculated as average values over three independent runs. Sulfur (and nitrogen) contamination in sample **13** is due to minor physisorbed residues of **3** in the blank sample.
- [22] According to elemental analysis results for sample **13**, we estimate a functionalisation loading of 0.635 mmol of  $-C_6H_4-N_3$  per gram of material.
- [23] a) A. Cui, X. Peng, J. Fan, X. Chen, Y. Wu, B. Guo, *J. Photochem. Photobiol. A* **2007**, *186*, 85–92; b) H. Lu, S. S. Zhang, H. Z. Liu, Y. W. Wang, Z. Shen, C. G. Liu, X. Z. You, *J. Phys. Chem. A* **2009**, *113*, 14081–14086; c) S. Mula, K. Elliott, A. Harriman, R. Ziesse, *J. Phys. Chem. A* **2010**, *114*, 10515–10522; d) A. Vázquez-Romero, N. Kielland, M. J. Arévalo, S. Preciado, R. J. Mellanby, Y. Feng, R. Lavilla, M. Vendrell, *J. Am. Chem. Soc.* **2013**, *135*, 16018–16021.
- [24] For both homo- and hetero-functionalisation, the amount of terminal alkynes was kept in excess with respect to the estimated azido groups available at the SWCNT sidewalls ( $\approx 5:1$ ).
- [25] C. F. Chiu, N. Dementev, E. Borguet, *J. Phys. Chem. A* **2011**, *115*, 9579–9584 and refs. cited therein.
- [26] M. S. Strano, C. A. Dyke, M. L. Usrey, P. W. Barone, M. J. Allen, H. Shan, C. Kittrell, R. H. Hauge, J. M. Tour, R. E. Smalley, *Science* **2003**, *301*, 1519–1522.
- [27] M. R. Heinrich, *Chem. Eur. J.* **2009**, *15*, 820–833.
- [28] P. Salice, E. Fabris, C. Sartorio, D. Fenaroli, V. Figà, M.-P. Casaletto, S. Cataldo, B. Pignataro, E. Menna, *Carbon* **2014**, *74*, 73–82.
- [29] Similar fluorescence lifetimes (ranging from 3.0 to 3.14 ns) have been recently reported for related BODIPy derivatives in  $CH_2Cl_2$ ; see: S. Mula, G. Ulrich, R. Ziesse, *Tetrahedron Lett.* **2009**, *50*, 6383–6388.
- [30] J. A. Prescher, C. R. Bertozzi, *Nat. Chem. Biol.* **2005**, *1*, 13–21.
- [31] D. D. Perrin, W. L. F. Armarego, D. R. Perrin, *Purification of Laboratory Chemicals, Vol. 1, 2nd ed.*, Pergamon, Oxford, New York, **1980**.
- [32] E. Maligaspe, N. V. Tkachenko, N. K. Subbaiyan, R. Chitta, M. E. Zandler, H. Lemmetyinen, F. D'Souza, *J. Phys. Chem. A* **2009**, *113*, 8478–8489.
- [33] M. J. Leonardi, M. R. Topka, P. H. Dinolfo, *Inorg. Chem.* **2012**, *51*, 13114–13122.

Received: November 11, 2014

Published online on ■ ■ ■, 0000

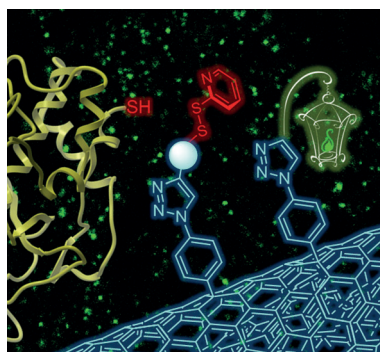
## FULL PAPERS

G. Tuci, L. Luconi, A. Rossin, F. Baldini,  
S. Cicchi, S. Tombelli, C. Trono,  
A. Giannetti, I. Manet, S. Fedeli, A. Brandi,  
G. Giambastiani\*

■■■ – ■■■



**A Hetero-Bifunctional Spacer for the  
Smart Engineering of Carbon-Based  
Nanostructures**



**Building on solid foundations:** A hetero-bifunctional linker joining a “cleavable” disulfide moiety and a “clickable” terminal acetylene group was synthesized and used to decorate carbon nanotubes (CNTs). When used in combination with other selected terminal acetylene molecules, the linker can impart multimodality through a controlled click reaction to give carbon nano hybrids (see figure).